Progress In Electromagnetics Research C, Vol. 124, 111–124, 2022

Ringing Phenomenon-Based Circularly Polarized MIMO Antenna for Ku/K Band Communication

Aditya K. Singh*, Amrees Pandey, Sweta Singh, Vandana Yadav, Ram S. Yadav

Abstract—A compact size UWB circularly polarized (CP) dual-port MIMO antenna is designed for Ku/K band applications. The proposed antenna contains a revised circle-shaped slot from the radiation patch on the front-side and a stepped-feed line on the back-side of the substrate. The orthogonal position of the antenna ports allows us to produce isolation of more than 30 dB and has a (−10 dB) impedance bandwidth of 68% (14.3–29.3 GHz) at two resonant frequencies 15.6 GHz and 24.7 GHz, respectively. 3 dB ARBW in the operating bands is 14.6% and 6.7%, respectively. The total size of the MIMO antenna is $0.1\lambda \times 0.05\lambda \times 0.003\lambda\,\text{mm}^3$ at a lower frequency. Diversity characteristics like ECC, DG, TARC, & CCL are determined to confirm the MIMO antenna's work qualities. Ringing resonating frequencies are observed at lower operating bands and are responsible for gain degradation. The proposed antenna has excellent characteristics for satellite and NASA's Tracking Data Relay Satellite application.

1. INTRODUCTION

Multiple-input multiple-output (MIMO) technology has attracted astonishing attention due to its advance data rate and channel capacity [1, 2]. The demand of ultra-wideband (UWB) technologies has increased with high data rate, low cost, & broad communication capacity. However, there were some problems of multipath fading & reliability. To resolve this problem, MIMO technology has been a solution [3]. To improve the properties of antenna such as transmission rate and channel capacity, UWB technology is combined with MIMO although there is big problem of multipath fading [4]. In addition to, it can also enhance communication quality and efficiency at the same time. UWB & MIMO technologies are combined through space multipath & parallel transmission of several signals, and appreciable multiplexing and diversity benefits can be conclude X, K, and Ka bands with broad applications [2, 5]. Additionally, the problems inherent in constructing MIMO antennas include developing densely packed antenna parts with low mutual coupling and good isolation, which increases the antenna's performance [6]. The big challenge for researchers is to maintain the best balance between miniaturization and high isolation. Under this investigation a number of UWB-MIMO antennas have been considered by the researchers [7–9]. Additionally, antennas with circular polarization (CP) show a lot of significant advantages regarding signal propagation in comparison to linear polarization (LP), as circularly polarized antennas are able to lessen multipath interference remarkably and are inconsistent with the orientation of the transmitting and receiving antennas. In the literature to increase the isolation, axial ratio bandwidth (ARBW) and impedance bandwidth of a UWB-MIMO antenna, a number of methods have been described. In [10], Saini and Dwari described an inverted-L planar strip ground plane to obtain a wide ARWB by feeding a conventional coplanar waveguide (CPW) into a square MIMO antenna [11], a CP-MIMO antenna mounted on an L-Strip dielectric resonator for WLAN application. Next, Sharma et al. considered a T-shape metallic feed line with a circular patch to achieve good isolation of over 20 dB for wireless communication [12]. According to Le and Yun, a

Received 30 July 2022, Accepted 7 September 2022, Scheduled 20 September 2022
* Corresponding author: Aditya Kumar Singh (aditya08129@gmail.com).
The authors are with the Department of Electronics & Communication, University of Allahabad, Prayagraj, India.

corner-fed square-ring radiator is designed through a rhombic shaped slot and an inverted V-shape. Extra parasitic ports are probed to obtain the CP wave [13]. The authors in [14] designed a reflector antenna for a circularly polarized Ku/K band feed system. Moreover, Singh et al. explained a hammer shape radiating patch with quad-port circular polarization for K band application [15]. Similarly, a super wideband MIMO antenna for S, C, X, K, & Ka bands is examined for wireless communication by Krishna et al. [16]. The authors in [17] proposed four identical hexagon-shaped slotted ground planes and microstrip line feeds designed for the fifth-generation millimeter-wave applications. The diversity characteristics of a MIMO antenna system are discussed and compared with reported literature, shown in Table 1. Compared to other MIMO antennas [17–23], the dimension of the discussed antenna is $25 \times 12.5 \times 0.8\,\text{mm}^3$ which is found to be very compact. Among the results, the proposed peak gain of the MIMO antenna is 5.2, 3.8 dBi apart from [21, 22]. Radiation efficiency and excellent isolation were found to be 98% and 33, 38, respectively, which are higher than other antennas.

Table 1. Comparison of the dual-port MIMO antenna designed with existing references in different aspects.

Dimension of Antenna (mm^3)	Number of antennas	Frequency Band (GHz)/ Impedance bandwidth (%)	Isolation (dB)	Average Efficiency (%)	Average Gain (dBi)	ECC	DG	CCL
$29.5 \times 60 \times 1.6$ [18]	2	3–20/42.4	23	80.2	3.7–4.2	0.001	9.99	0.32
$40 \times 40 \times 1.6$ [19]	4	3.3–13.75/122	18	89	5.5	0.012	9.998	0.2
$50 \times 40 \times 1.6$ [20]	2	2.5–11/125	15	69.2	2.11	0.01	NR	NR
$50 \times 30 \times 1.6$ [21]	2	2.5–14.5/141	20	NR	4.3	0.04	7.4	NR
$55.6 \times 50.5 \times 1.6$ [22]	2	1.5–40/185	20	NR	7.5	0.005	9.9	0.35
$30 \times 52 \times 1.6$ [23]	2	2.0–3.6/1.6, 6.6–7.9/1.3, 9.6–12.7/3.1, 11–15.6/4.6	−20, −40	NR	5, 3, 4.2, 6.6	0.024	9.9	0.23
$30 \times 30 \times 0.8$ [24]	2	3.08–10.9/112	20	NR	5	0.013	9.51	0.3
$25 \times 12.5 \times 0.8$ [Proposed]	2	14.3–29.3/68.4	33, 38	98	5.2,3.8	0.002	9.9	0.5

In the present article, the authors design a new modified circle-shaped UWB-MIMO antenna for Ku/K band application. Further, the size of the antenna printed on an RT-duroid 5880 substrate with $\varepsilon_{rsub} = 2.20$, $\tan\delta = 0.0009$, thickness of 0.8 mm is reduced ($25 \times 25\,\text{mm}^3$) with highly mutual coupling characteristics, enhanced gain, & diversity performance as compared to reference antennas in Table 1. The main outcomes of the present investigation are as follows;

I. The proposed MIMO antenna design is small, cost-effective with its fabricated structure, and the various simulated results are supported by the measurable results of various optimized parameters of the antenna.

II. The dual-port circularly polarized MIMO antenna is offered with the aid of an orthogonal placement, i.e., impedance bandwidth of 68% (14.3–29.3 GHz), and the isolation between ports is greater than −33 dB and −38 dB at two resonant frequencies 15.6 GHz and 24.7 GHz, respectively.

III. The ringing effect is achieved in the operating band (14.3–29.3 GHz). This unique effect makes this work novel, which is elaborately described in the result section.

2. ANTENNA DESIGN, FABRICATED ARCHETYPE AND ANALYSIS

This circularly polarized dual-port MIMO antenna is designed and simulated using ANSYS HFSS 16.2 simulator. Simulated and fabricated antennas using RT-duroid 5880 with $\varepsilon_{rsub} = 2.20$, $\tan\delta = 0.0009$, and thickness of 0.8 mm are shown in Figures 1(a)–(b) & antenna under anechoic chamber and test condition using VNA E5072C (cf. Figures 2(a)–(b)).

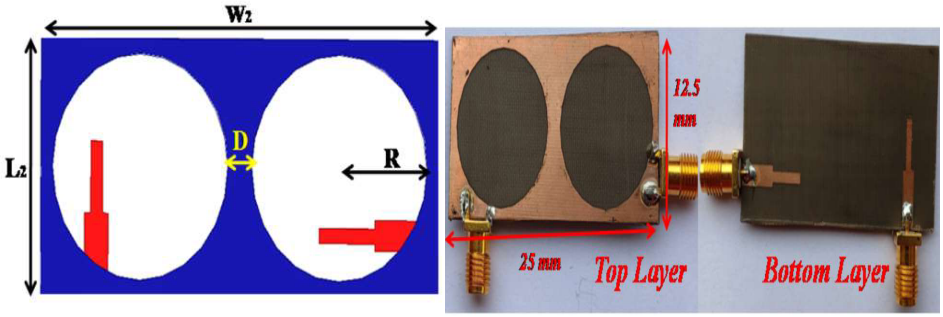

(a) (b)

Figure 1. (a) Top (circular patch) and bottom (Stepped feed line) see the layout of the proposed antenna. (b) Fabricated prototype (top-layer & bottom-layer).

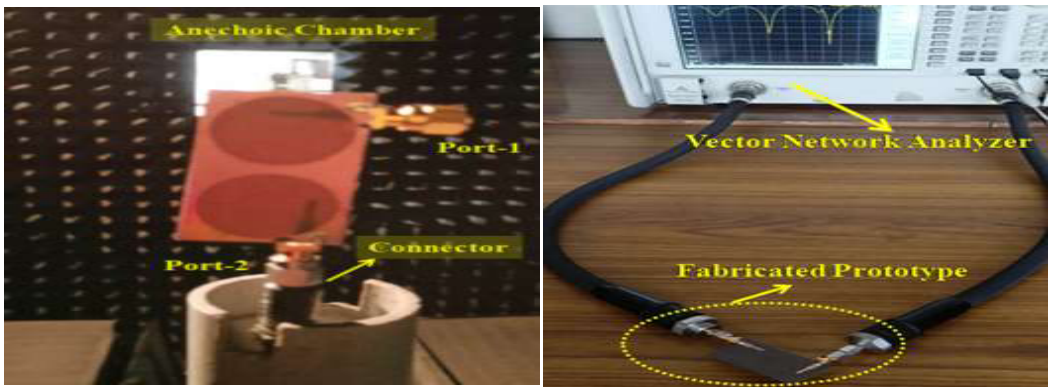

(a) (b)

Figure 2. (a) Antenna measurement using anechoic chamber. (b) Measurement setup using VNA E5072C.

2.1. Development of Antenna Design

Dual-port circularly polarized MIMO antenna evolution is shown in three stages as in Figure 3. The dimensions of each antenna (A_1–A_3) are well labeled in Table 2. The inter-element spacing of $D = 1$ mm creates a circular radiating patch. Stepped feed lines provide excellent impedance matching along with isolation between elements. The development of the proposed MIMO antenna geometry (A_1–A_3) has been examined (cf. Figure 3) with a single port and dual ports in terms of return loss, isolation, peak gain, and axial ratio characteristics which are presented in Figures 4, 5, 6, 7, and 8, respectively.

2.1.1. Single-Port Probe

Figure 2 illustrates the single port (A_1) antenna that has an overall size of $12.5 \times 12.5 \times 0.8\,\text{mm}^3$, and optimized measurements of the antenna are shown in Table 2. The single port structure in the first phase is inspired by a stepped feed line. Additionally, UWB is attained by etching the circular ring

Table 2. Optimized dimensions of considered antenna (mm).

Parameters	Dimensions (mm)
L_1, W_1 (Single Port-length & width)	12.5, 12.5
L_2, W_2 (dual port-length & width)	12.5, 25
X_1, Y_1 (Feed length & width)	10, 1.5
X_2, Y_2 (Feed length & width)	8, 3
D (Distance between circular rings)	1
R (Radius of circular rings)	11
S (Shift of circular rings)	5.5

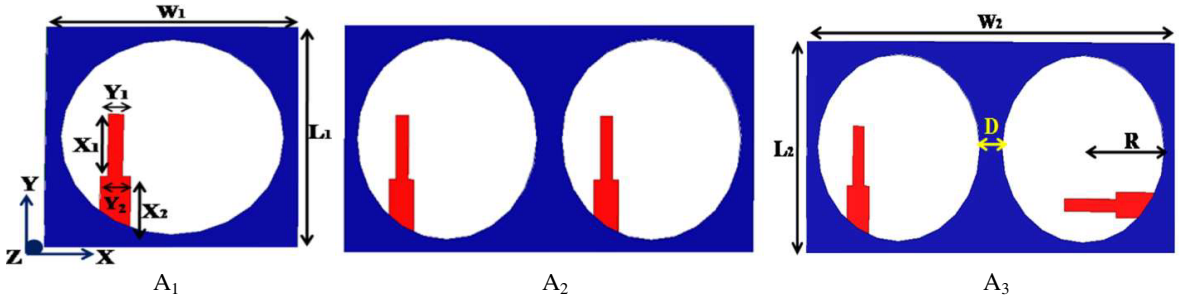

Figure 3. Geometrical configuration of proposed antenna (A_1, A_2 and A_3).

from the radiating rectangular patch and placing the stepped feed in an optimized location. From Figure 4(a), a variation in $|S_{11}|$ is perceived by etching out the square-, triangle-, and circle-shaped slots from the radiating patch. After that, analysis of the variation in radius R of the circular slot is accomplished to examine the change in impedance bandwidth. From Figure 4(b), it is clear that at $R = 11$ mm, maximum impedance bandwidth is obtained. Finally, the phase is designed in a manner that the maximum value of the bandwidth is obtained for $S = 5.5$ mm, and the positional variation of the phase feed is obtained through a step of "S" size 3 mm (cf. Figure 4(c)). The dual operating bands ($|S_{11}| \leq -10$ dB) of this antenna are attained within 14.3–16.3 GHz & 22.2–31.4 GHz, respectively.

2.1.2. Dual-Port Probe

A dual-port MIMO antenna is installed for single port antennas via dual-port parallel and orthogonal orientation probes.

2.1.2.1. Parallel Orientation

The suggested dual-port circularly polarized MIMO antenna is projected in parallel. Return loss $|S_{11}|$ performance is perceived under three different steps: Step 1: single-port, Step 2: dual-ports with parallel placement in relation to single-port antennas (c.f. Figure 5(a)), and it is proved that $|S_{11}|$ is roughly the same in both steps. The method of parallel stepped feed line is used at the bottom to achieve minimum isolation (< -26 dB) and (< -25 dB) at two resonant frequencies, 15.6 GHz and 24.7 GHz, respectively, over the entire frequency band, which is presented in Figure 5(b).

2.1.2.2. Orthogonal Orientation

Due to their orthogonal orientation, the dual ports return losses (14.3–29.3 GHz) with an impedance bandwidth of 68% & gain of 5.8 dBi and 4.2 dBi at two resonant frequencies at 15.6 GHz and 24.7 GHz, respectively, are shown in Figure 6(a). The second important outcome is that the isolation between two ports exceeds -33 dB and -38 dB at two resonant frequencies, 15.6 GHz and 24.7 GHz, respectively, over

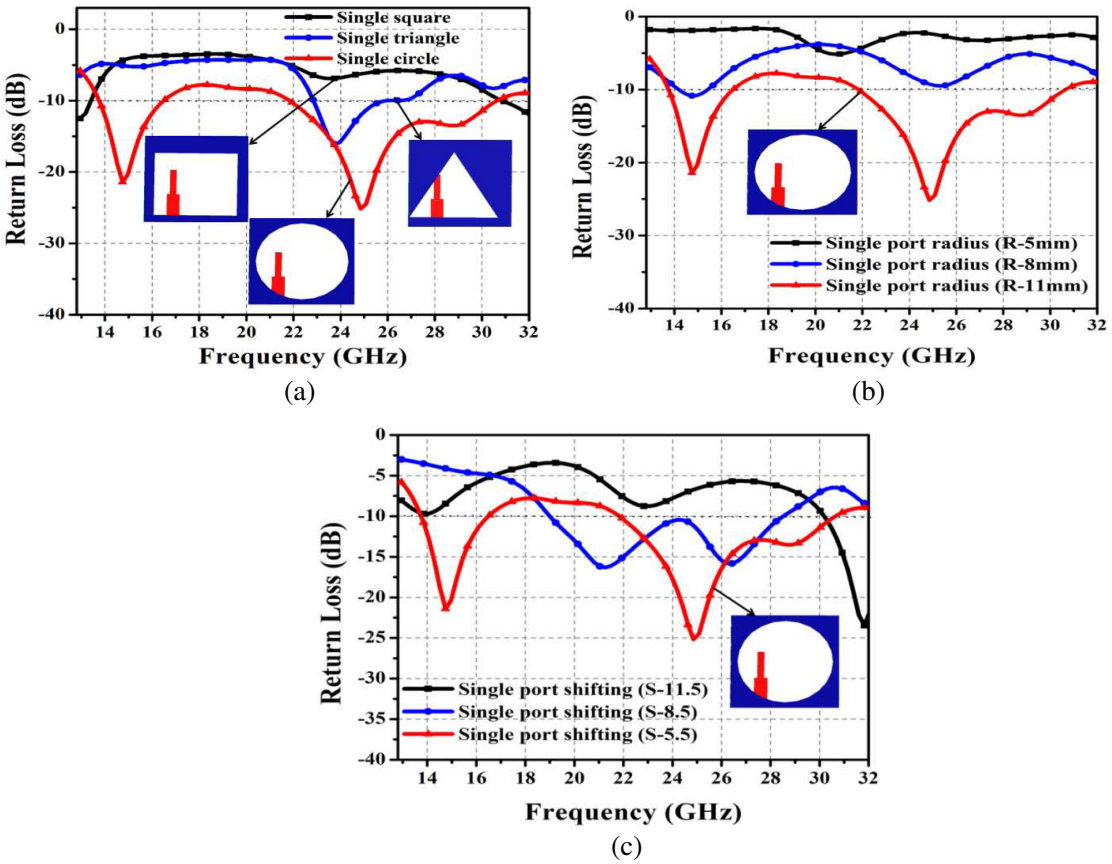

Figure 4. The variation of $|S_{11}|$ for different analysis. (a) Slots shapes. (b) Radius of circular slot $R = 11\,\text{mm}$. (c) Shifting stepped feed ($S = 5.5\,\text{mm}$).

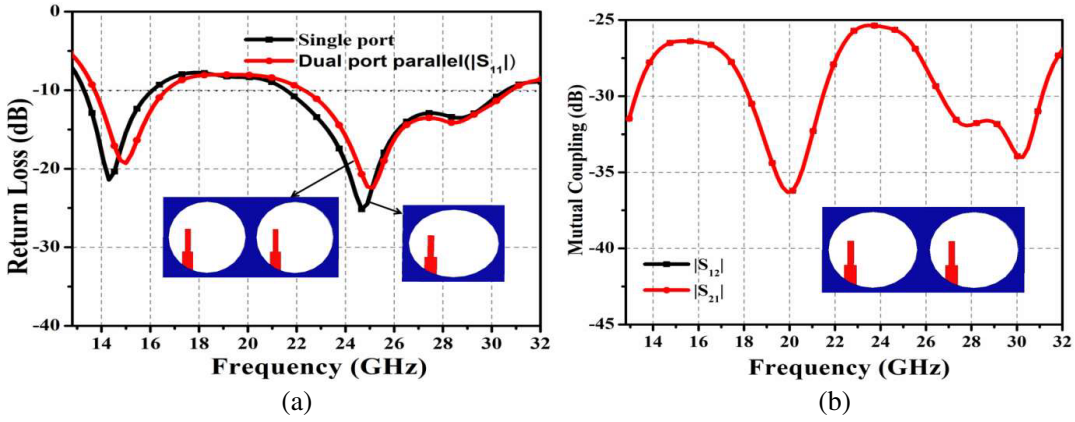

Figure 5. (a) Return Loss single port & Dual port parallel placement. (b) Mutual coupling in parallel placement.

the total frequency band, as shown in Figure 6(b). These radiating elements achieve excellent ultra-wideband and isolation (14.3–29.3 GHz) characteristics. Furthermore, the proposed structure shows 3-dB ARBW for the entire operating bandwidth (c.f. Figure 6(c) and Table 2). We explore the ringing effect, when two resonant frequencies (15.6 GHz and 24.7 GHz) are obtained in the single-band known as "ringing resonant frequencies". We also observe that the peak gain at the first resonant frequency

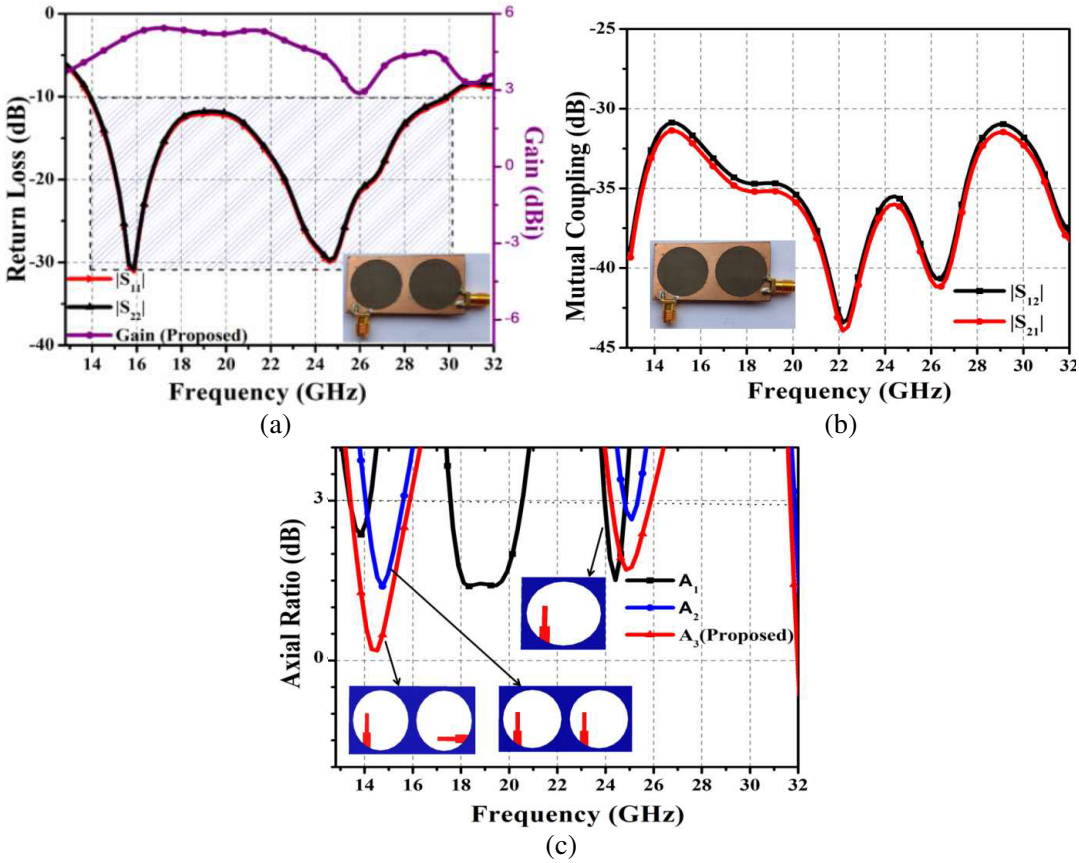

Figure 6. Simulated (a) $|S_{11}|$ of dual ports in orthogonal placement. (b) Isolation in orthogonal placement. (c) Axial ratio of A_1, A_2 & A_3.

(15.6 GHz) is higher than that at the following ringing resonant frequency (24.7 GHz). A decrease in gain is observed at the second ringing resonant frequency, and it is clear that the ringing phenomenon reduces the antenna performance (c.f. Figure 6(a)) [25].

3. EXPERIMENTAL RESULTS & DISCUSSION

3.1. IBW (Impedance Bandwidth)

This proposed model (S-parameter) is simulated, fabricated, and tested which is measured using VNA E5072C. Figure 7(a) shows simulated and measured return losses $|S_{11}|$ & $|S_{22}|$ of the proposed (A_3) antenna. The $|S_{11}|$ (measured) has single resonating bands of impedance BW of 14.7 GHz (14.1–28.8 GHz), and $|S_{22}|$ has the same behavior as $|S_{11}|$. Both show UWB characteristics, throughout the desired frequency bands. However, the results (simulated & measured) are in decent agreement except for an insignificant mismatch due to human errors and tolerances in the fabrication process and soldering. From the survey of Figure 7(b), it has been suggested that the antenna topology provides more than −30 dB isolation −33 dB (measured) & −38 dB (simulated) between the antenna elements for the proposed configurations, making it appropriate for dual circularly polarized MIMO antenna. Figure 7(a) depicts that the two resonating frequencies in a single band could be termed as "ringing resonant frequency". We observe that peak gain at the first resonant frequency (15.6 GHz simulated and 16.1 GHz measured) of the "ringing resonant frequency" is higher than the second ringing resonant frequency (24.7 GHz simulated and 24.3 GHz measured). A decrease in gain (cf. Figure 6(a)) is observed at the second ringing resonant frequency which suggests that the ringing phenomenon degrades the antenna performance. The gain, however, increases marginally with the beginning of the cycle at the

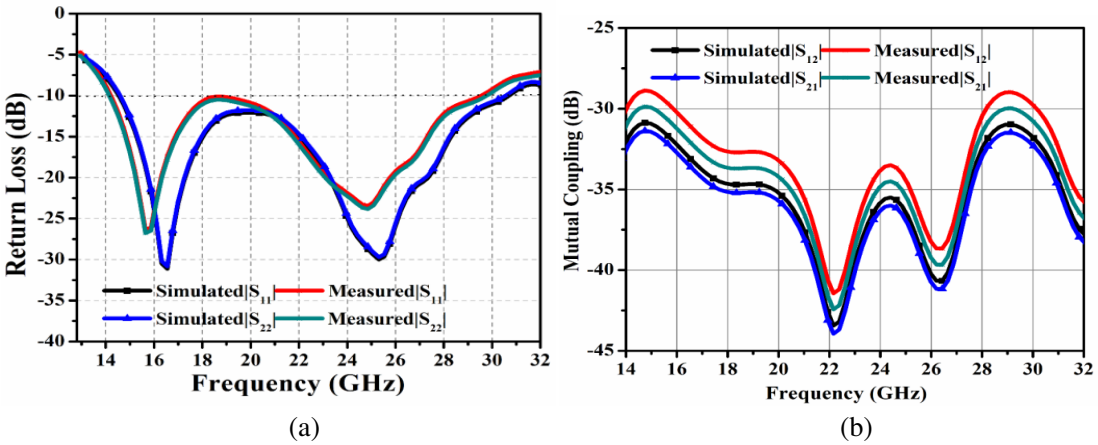

Figure 7. Simulation and measured. (a) Return loss. (b) Isolation.

second ringing resonant frequency, but fails to yield a gain similar to or close to the value obtained at the first ringing resonant frequency [25].

3.2. Axial Ratio, Radiation Efficiency and Peak Gain

Figure 8(a) and Table 3 demonstrate the axial ratio plots (simulated & measured) of circularly polarized antenna which covers the resonance frequencies at 15.6 GHz and 24.7 GHz, respectively. Figure 8(b) clearly demonstrates the radiation efficiency (simulated) and gain (simulated and measured) with the variation of frequency band. The radiation efficiency of the considered antenna is more than 98%, and total efficiency takes ohmic losses and impedance mismatch into account. The radiation efficiency (η) of considered antenna is calculated by the given Equation (1) (cf. Figure 8(b)).

$$\eta = \frac{Gain}{Directivity} \times 100\% \tag{1}$$

The measured peak gains are about 5.2 dBi (simulated), 4.9 (measured) & 3.8 dBi (simulated), 2.7 (measured) at two resonant frequencies 15.6 GHz and 24.7 GHz respectively over the entire frequency band in Figure 8. The circular polarization attributes of the presented dual-port MIMO & its performance can be better known with the help of Table 3 in terms of BW, % IBW & % IARBW.

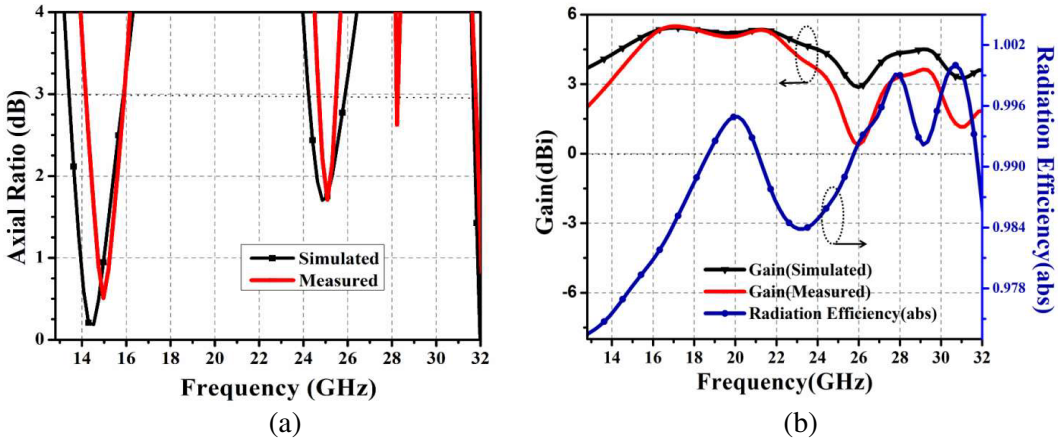

Figure 8. (a) Axial ratio (simulated & measured). (b) Gain (simulated & measured) and simulated radiation efficiency.

Table 3. Comparative performance analysis of antennas (A_1, A_2 and A_3).

Antenna	Resonating bands (GHz)/BW (GHz)	% IBW	ARBW (GHz)	% IARWB
A_1 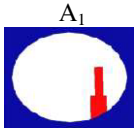	(14.3–16.3) /2	13.07	14.1–15.3/1.2	8.1
	(22.2–31.4)/9.2	34.3	24.8–25.2/0.4	1.6
A_2 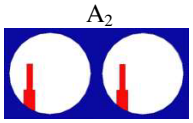	(14.5–16.8)/2.3	14.69	14.3–15.7/1.4	9.3
	(22.8–31.4)/8.6	31.7	24.5–24.8/0.3	1.2
A_3 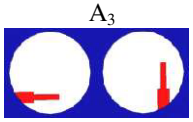	(14.3–29.3) /15(S)	68.4(S)	13.9–16.1/2.2(S) 14.3–16.1/1.8(M)	14.6(S) 11.8(M)
	(14.1–28.8)/14.7(M)	68.1(M)	24.2–25.9/1.7(S) 24.3–25.3/1 (M)	6.7(S) 4.0(M)
Bandwidth: BW, Impedance Bandwidth: IBW, Axial Ratio Bandwidth: ARBW, Impedance Axial Ratio Bandwidth: IARBW, Simulated: S, Measured: M.				

3.3. Performance Parameter

In this section, to validate the MIMO-CP antenna, various parameters such as the envelope correlation coefficient (ECC), diversity gain (DG), total active reflection coefficient (TARC), & channel capacity loss (CCL) are used. All are explained in the following section.

3.3.1. Envelop Correlation Coefficient (ECC)

Envelope correlation coefficient (ECC) is a vital parameter which measures the degree of correlation and isolation in communication channels [26]. It can be derived with two methods: (i) with the help of S-parameters in the Equation (2) [27] & (ii) using far-field radiation characteristics in Equation (3) [28]. ECC derived from the radiation patterns in a multiple-antenna system measures how much the radiation pattern of one antenna element affects the radiation patterns of another antenna elements. Equation (2) is also used to calculate ECC which is up to 0.002, thus it can be practically tolerable for MIMO applications in this paper (in Figure 9(a)).

$$ECC = \frac{|S_{11} * S_{12} + S_{21} * S_{22}|}{(1 - |S_{11}^2| - |S_{21}^2|)(1 - S_{22}^2| - |S_{12}^2|)} \tag{2}$$

$$ECC_F = \frac{\left| \iint\limits_{4\pi} \left[E_i(\theta, \phi) * E_j(\theta, \phi) \right] d\Omega \right|^2}{\iint\limits_{4\pi} |E_i(\theta, \phi)|^2 \, d\Omega \iint\limits_{4\pi} |E_j(\theta, \phi)|^2 \, d\Omega} \tag{3}$$

3.3.2. Diversity Gain (DG)

DG is the process as soon as transmitters accept the form of a transmission current through different channel paths, with the results of the variation often being complete. Its value in terms of good diversity performance is found close to 10 dB. DG can be computed by using Equation (3) from the ECC [29]

$$Diversity\ Gain = 10 \times \sqrt{1 - (ECC)^2} \tag{4}$$

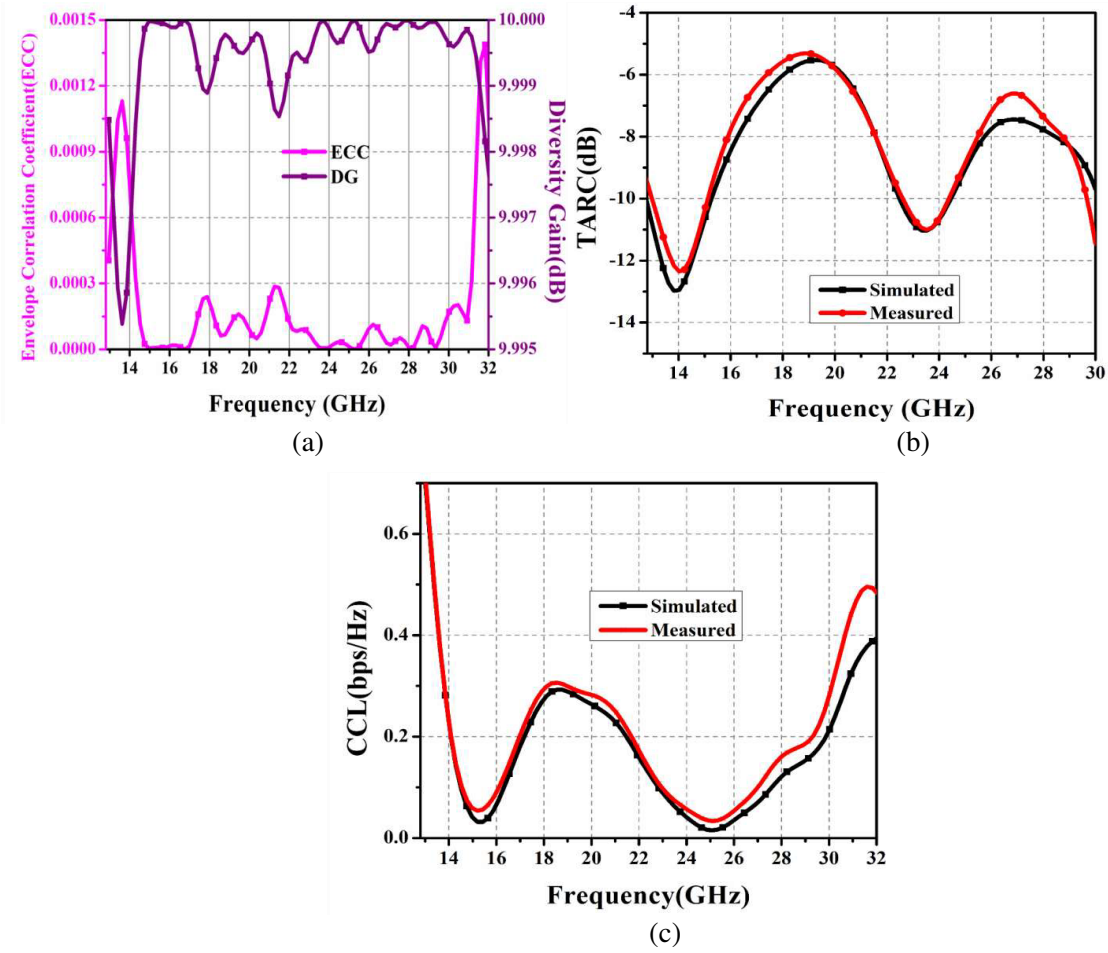

Figure 9. Proposed MIMO antenna. (a) ECC & DG plots. (b) TARC (simulated & measured). (c) CCL (simulated & measured).

The proposed design shows DG value above 9.98 which also covers the resonant frequencies of 15.6 GHz and 24.7 GHz respectively (in Figure 9(a)).

3.3.3. Total Active Reflection Coefficient (TARC)

It is an important factor in determining bandwidth and to better understand the diversity characteristics of a dual-port antenna. It shows the ratio of the square root of the reflected power to the incident power, and it is calculated by Equation (5) [30]. As depicted in Figure 9(b), it is simulated and measured in an ideal case with TARC value less than −10 dB for MIMO antenna.

$$\Gamma_a^t = \frac{\sqrt{\Sigma_i^N |b_i|^2}}{\sqrt{\Sigma_i^N |a_i|^2}} \tag{5}$$

where b_i — Reflected waves & a_i — Incident waves. Afterwards, MIMO antenna performance by S-parameter cannot be expected for dual-port antenna by Equation (6) [31].

$$TARC = \frac{\sqrt{(S_{11} + S_{12})^2 + (S_{22} + S_{21})^2}}{\sqrt{2}} \tag{6}$$

3.3.4. Channel Capacity Loss (CCL)

For MIMO configuration, a message can be sent repeatedly in a communication system when the CCL metric expresses the maximum rate. It is calculated by using Equation (7) [32].

$$\begin{aligned} CCL &= -\log_2 \det \begin{pmatrix} a_{11} & a_{12} \\ a_{21} & a_{22} \end{pmatrix} \\ a_{11} &= 1 - \left(|S_{11}|^2 + |S_{12}|^2 \right) \\ a_{22} &= 1 - \left(|S_{22}|^2 + |S_{21}|^2 \right) \\ a_{12} &= -\left(S_{11}^* S_{12} + S_{21}^* S_{12} \right) \\ a_{21} &= -\left(S_{22}^* S_{21} + S_{12}^* S_{21} \right) \end{aligned} \tag{7}$$

As seen in Figure 9(c), the best diversity performance in terms of the proposed antenna CCL should be within the permissible range for the specified frequency band up to 0.5 bit/s/Hz (simulated and measured).

3.3.5. Surface Current Distribution & Radiation-Pattern

The presented MIMO antenna exhibits circularly polarized characteristics, and circularly polarized antenna analysis using surface current distribution is demonstrated in in Figure 10 for the phases 0°, 90°, 180°, and 270° at resonant frequency 15.6 GHz. At phase 0°, it is found that the direction of the arrows shows the orientations of the dominant field components at different angular time intervals. As a result, the current vectors are located in $-x$-direction predominantly whereas at phase 180°, the dominant current vectors are located in $+x$-direction. At phases 90° and 270°, the field distributions are opposite and magnitudes in phase. It is seen that the current vectors changing with time move in a clockwise direction. Hence, it is clear that the polarization of this topology is left-hand circularly polarized (LHCP). Figure 11 clearly shows that the considered antenna exhibits right-hand circular polarization (RHCP) for resonant frequency 24.7 GHz. From 0° to 270°, the field distribution changes with the difference in phases. At phase 0°, the current is predominantly located in the $-x$-direction whereas at phase 180°, the dominant current vectors are in the $+x$-direction. The field distributions at phases 90° & 270° are opposite and magnitudes in phase. As can be noticed, the current vectors,

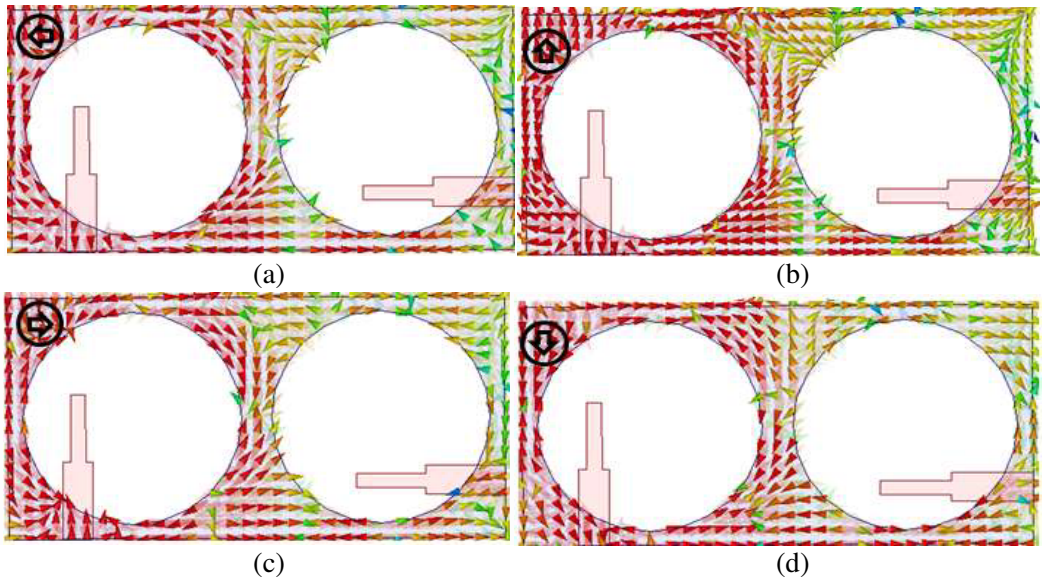

Figure 10. Electric field distribution at 15.6 GHz. (a) wt = 0°. (b) wt = 90°. (c) wt = 180°. (d) wt = 270°.

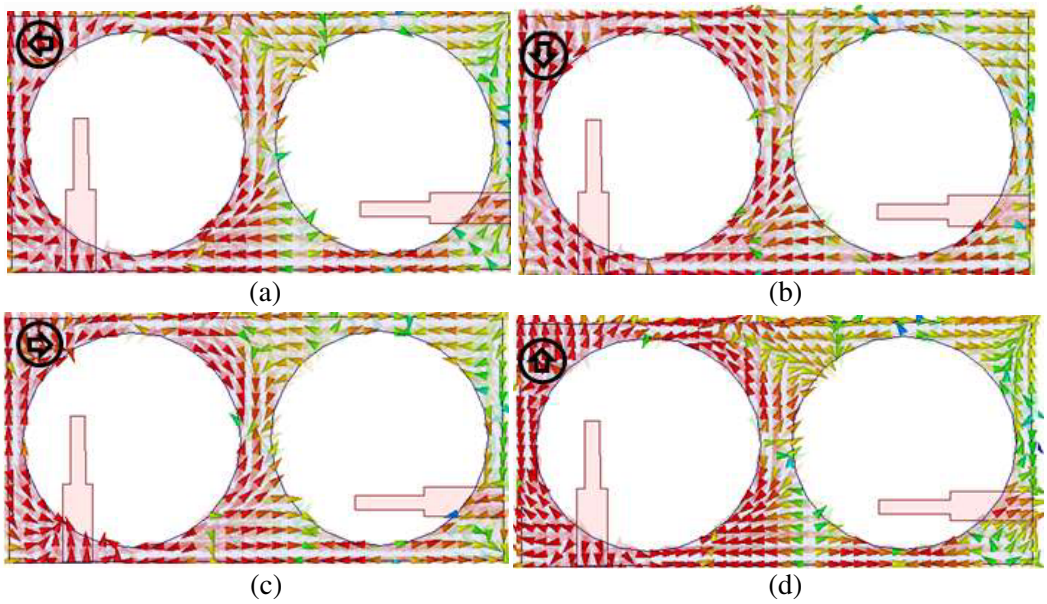

Figure 11. Electric field distribution at 24.7 GHz. (a) wt = 0°. (b) wt = 90°. (c) wt = 180°. (d) wt = 270°.

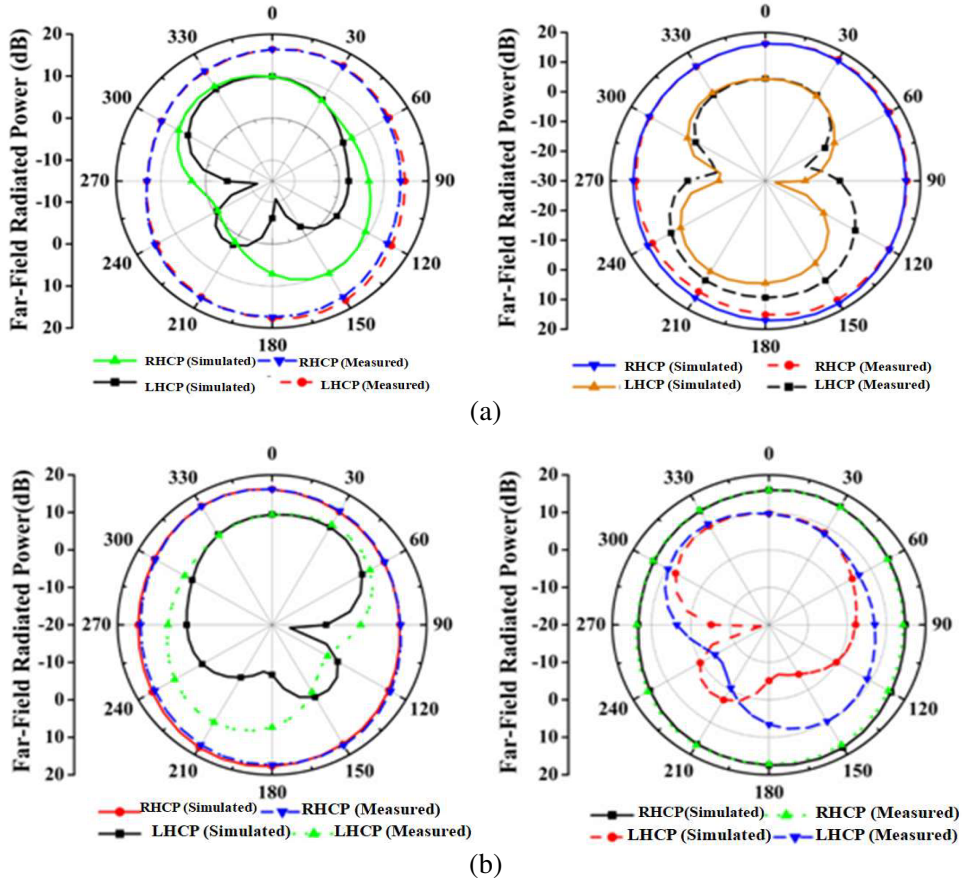

Figure 12. Measured & simulated radiation-pattern at (a) 15.6 GHz, (b) 24.7 GHz.

diversifying with time, are rotating in a counterclockwise direction. Figure 12(a) shows the radiation patterns (simulated & measured) of the circularly polarized dual-port MIMO antenna at the resonating frequency 15.6 GHz, when port-1 is excited. It can be seen that in both planes 0° and 90°, the antenna is pointed in the z-direction of LHCP operation. Similarly, the radiation-pattern (simulated and measured) of a circularly polarized dual-port MIMO antenna at 24.7 GHz resonance frequency is observed, when port-2 is excited. In In Figure 12(b), it can be noticed that at 0° and 90° in both planes, the antenna indicates RHCP operation. The anechoic chamber's aiding tool & small inconsistencies in test results may result in inaccuracies of the obtained gain in the antenna used for the study. While there are some discrepancies in the observed radiation patterns, UWB-MIMO antennas are supportable and important for K and Ku band applications.

4. CONCLUSION

A compact CP-dual port MIMO antenna is modeled, analyzed, investigated, and fabricated for Ku/K band applications. The considered MIMO antenna has a UWB of impedance bandwidth 68% (14.3–29.3 GHz) at two resonant frequencies 15.6 GHz and 24.7 GHz, respectively. The excellent isolation (greater than −33 dB and −38 dB) is achieved by etching circle-shaped slots from the radiating patch. Moreover, the ringing effect have been observed to reduce the antenna's peak gain over the low-frequency band (20.3–29.3 GHz) and at a higher frequency band (14.3–20.3 GHz), and negligible variation in the ringing effect gain is reported. The proposed dual port, small sized ($0.1\lambda \times 0.05\lambda \times 0.003\lambda\,\mathrm{mm}^3$) antenna shows that a measured 3-dB axial ratio with a relatively UWB of 14.6% (13.9–16.1 GHz), 6.7% (24.2–25.9 GHz) is distinctively better than previously proposed CP antennas [33, 34].

REFERENCES

1. Liang, C., R. Su, P. Gao, and P. Wang, "Compact printed MIMO antenna with 6.1 GHz notched band for ultra-wideband applications," *Progress In Electromagnetics Research Letters*, Vol. 76, 77–83, 2018.
2. Biswal, S. P. and S. Das, "A compact printed ultra-wideband multiple-input multiple-output prototype with band-notch ability for WiMAX, LTEband43, and WLAN systems," *International Journal of RF and Microwave Computer-Aided Engineering*, Vol. 29, No. 6, e21673, 2019.
3. Nouri, M. and S. A. Aghdam, "Reconfigurable UWB antenna with electrically control for triple on-demand rejection bandwidth," *Microwave and Optical Technology Letters*, Vol. 57, No. 8, 1894–1897, 2015.
4. Srivastava, K., S. Kumar, B. K. Kanaujia, and S. Dwari, "Design and packaging of ultra-wideband multiple-input-multiple-output/diversity antenna for wireless applications," *International Journal of RF and Microwave Computer-Aided Engineering*, Vol. 30, No. 10, e22357, 2020.
5. Gill, H. S., S. S., M. Singh, and G. Kaur, "Design of single-band MIMO antenna for Ku-band applications," *2019 International Conference on Electrical, Electronics and Computer Engineering (UPCON)*, 1–5, IEEE, 2019.
6. Khan, M. S., A. Iftikhar, R. M. Shubair, A. D. Capobianco, B. D. Braaten, and D. E. Anagnostou, "A four element, planar, compact UWB MIMO antenna with WLAN band rejection capabilities," *Microwave and Optical Technology Letters*, Vol. 62, No. 10, 3124–3131, 2020.
7. Zhao, X., S. Riaz, and S. Geng, "A reconfigurable MIMO/UWB MIMO antenna for cognitive radio applications," *IEEE Access*, Vol. 7, 46739–46747, 2019.
8. Liu, Li, S. W. Cheung, and T. I. Yuk, "Compact MIMO antenna for portable devices in UWB applications," *IEEE Transactions on Antennas and Propagation*, Vol. 61, No. 8, 4257–4264, 2013.
9. Khan, M. I., M. I. Khattak, S. Ur Rahman, A. B. Qazi, A. A. Telba, and A. Sebak, "Design and investigation of modern UWB-MIMO antenna with optimized isolation," *Micromachines*, Vol. 11, No. 4, 432, 2020.
10. Saini, R. K. and S. Dwari, "A broadband dual circularly polarized square slot antenna," *IEEE Transactions on Antennas and Propagation*, Vol. 64, No. 1, 290–294, 2015.

11. Sahu, N. K., G. Das, and R. K. Gangwar, "L-shaped dielectric resonator based circularly polarized multi-input-multi-output (MIMO) antenna for wireless local area network (WLAN) applications," *International Journal of RF and Microwave Computer-Aided Engineering*, Vol. 28, No. 9, e21426, 2018.
12. Sharma, A., G. Das, and R. K. Gangwar, "Design and analysis of tri-band dual-port dielectric resonator based hybrid antenna for WLAN/WiMAX applications," *IET Microwaves, Antennas & Propagation*, Vol. 12, No. 6, 986–992, 2018.
13. Le, T. T. and T.-Y. Yun, "A quad-band dual-sense circularly-polarized square-ring antenna for multi-functional wireless applications," *IEEE Access*, Vol. 7, 149634–149640, 2019.
14. Song, H., Z. Liu, and Z. Yan, "Design of a circular polarized Ku/K-band feed system for reflector antenna," *2020 International Conference on Microwave and Millimeter Wave Technology (ICMMT)*, 1–3, IEEE, 2020.
15. Singh, A. K., A. Pandey, S. Singh, V. Yadav, and R. Singh, "Quad-port circularly polarized MIMO antenna for K band applications," *2021 6th International Conference on Communication and Electronics Systems (ICCES)*, 405–410, IEEE, 2021.
16. Krishna, Ch M., M. S. Prapoorna, K. T. S. Sai, and M. S. Teja, "Super wideband 1×2 MIMO antenna for advanced wireless communication," *Advances in Electrical and Computer Technologies*, 509–519, Springer, Singapore, 2021.
17. Singh, A. K., A. K. Dwivedi, C. Jha, S. Singh, V. Singh, and R. S. Yadav, "A compact MIMO antenna for 5G NR frequency bands n257/n258/n261 under millimeter-wave communication," *IETE Journal of Research*, 2022.
18. Ahmed, B. T. and I. F. Rodríguez, "Compact high isolation UWB MIMO antennas," *Wireless Networks*, Vol. 28, No. 5, 1977–1999, 2022.
19. Suresh, A. C. and T. S. Reddy, "A flower shaped miniaturized 4×4 MIMO antenna for UWB applications using characteristic mode analysis," *Progress In Electromagnetics Research C*, Vol. 119, 219–233, 2022.
20. Lin, G.-S., C.-H. Sung, J.-L. Chen, L.-S. Chen, and M.-P. Houng, "Isolation improvement in UWB MIMO antenna system using carbon black film," *IEEE Antennas and Wireless Propagation Letters*, Vol. 16, 222–225, 2016.
21. Iqbal, A., O. A. Saraereh, A. W. Ahmad, and S. Bashir, "Mutual coupling reduction using F-shaped stubs in UWB-MIMO antenna," *IEEE Access*, Vol. 6, 2755–2759, 2017.
22. Saxena, G., P. Jain, and Y. K. Awasthi, "High diversity gain super-wideband single band-notch MIMO antenna for multiple wireless applications," *IET Microwaves, Antennas & Propagation*, Vol. 14, No. 1, 109–119, 2020.
23. Bhatia, S. S. and N. Sharma, "Modified spokes wheel shaped MIMO antenna system for multiband and future 5G applications: Design and measurement," *Progress In Electromagnetics Research C*, Vol. 117, 261–276, 2021.
24. Biswal, S. P. and S. Das, "A lowprofile dual port UWB-MIMO/diversity antenna with band rejection ability," *Int. J. RF Microw. Comput. Aided. Eng.*, e21159, 2017.
25. Singh, A. K., S. Singh, A. Pandey, S. Singh, and R. Singh, "A compact wideband patch antenna with defected ground for satellite communication," *Information and Communication Technology for Competitive Strategies (ICTCS 2020)*, 513–521, Springer, Singapore, 2021.
26. Singh, A. K., S. K. Mahto, and R. Sinha, "Compact super-wideband MIMO antenna with improved isolation for wireless communications," *Frequenz*, Vol. 75, Nos. 9–10, 407–417, 2021.
27. Blanch, S., J. Romeu, and I. Corbella, "Exact representation of antenna system diversity performance from input parameter description," *Electronics Letters*, Vol. 39, No. 9, 705–707, 2003.
28. Dwivedi, A. K., A. Sharma, A. K. Singh, and V. Singh, "Quad-port ring dielectric resonator based MIMO radiator with polarization and space diversity," *Microwave and Optical Technology Letters*, Vol. 62, No. 6, 2316–2327, 2020.

29. Chandel, R., A. K. Gautam, and K. Rambabu, "Design and packaging of an eye-shaped multiple-input–multiple-output antenna with high isolation for wireless UWB applications," *IEEE Transactions on Components, Packaging and Manufacturing Technology*, Vol. 8, No. 4, 635–642, 2018.
30. Manteghi, M. and Y. Rahmat-Samii, "Multiport characteristics of a wide-band cavity backed annular patch antenna for multipolarization operations," *IEEE Transactions on Antennas and Propagation*, Vol. 53, No. 1, 466–474, 2005.
31. Addepalli, T. B. and V. R. Anitha, "Design and parametric analysis of hexagonal shaped MIMO patch antenna for S-band, WLAN, UWB and X-band applications," *Progress In Electromagnetics Research C*, Vol. 97, 227–240, 2019.
32. Chatterjee, A., M. Midya, L. P. Mishra, and M. Mitra, "Dual-element multiple-input-multiple-output system for sub-6 GHz (5G) and WLAN applications with enhanced isolation," *Progress In Electromagnetics Research M*, Vol. 103, 197–207, 2021.
33. Baek, J. G. and K. C. Hwang, "Triple-band unidirectional circularly polarized hexagonal slot antenna with multiple L-shaped slits," *IEEE Transactions on Antennas and Propagation*, Vol. 61, No. 9, 4831–4835, 2013.
34. Ta, S. X., I. Park, and R. W. Ziolkowski, "Circularly polarized crossed dipole on an HIS for 2.4/5.2/5.8-GHz WLAN applications," *IEEE Antennas and Wireless Propagation Letters*, Vol. 12, 1464–1467, 2013.